Int J Thermophys (2013) 34:1398–1404
DOI 10.1007/s10765-013-1462-7

Features of the Frequency- and Time-Domain Photoacoustic Modalities

B. Lashkari · A. Mandelis

Received: 16 February 2012 / Accepted: 13 May 2013 / Published online: 6 July 2013

Abstract This article presents an instrumentation and modality-based study of the salient differences between pulsed and frequency-domain photoacoustic (PA) signals with respect to signal processing and imaging properties. The parameters of both modalities were adjusted to achieve the maximum signal-to-noise ratio (SNR). Experiments were performed by employing a dual-mode PA system and under the condition of maximum permissible exposure for both modalities. In addition, proper filtering has been applied post-processing to enhance the image quality for both methods. Theoretical estimates versus practical issues are discussed. In conclusion, it has been shown that parameters of these two methods can be adjusted to provide a competitive SNR and resolution.

Keywords Frequency-domain · Photoacoustic imaging · Photoacoustics · Pulsed laser photoacoustics

1 Introduction

Laser-induced ultrasound or photoacoustics (PA) has found many merits and applications in biomedical imaging and diagnosis. Most of these efforts employ nanosecond pulsed lasers as excitation sources which is referred to as time-domain (TD) PA. The alternative approach is to use a continuous wave laser with intensity modulation or coded excitation [1,2]. A fundamental study has been performed to estimate the ultimate sensitivity of a TD-PA system for the purpose of cancer tumor diagnosis [3].

B. Lashkari · A. Mandelis (✉)
Center for Advanced Diffusion-Wave Technologies (CADIFT), Department of Mechanical and Industrial Engineering, University of Toronto, Toronto, ON M5S 3G8, Canada
e-mail: ijt@mie.utoronto.ca

Previously, few authors compared the two PA modalities. They provided experimental comparisons on maximum depth detectivity and axial resolution, as well as some estimates of achievable SNR for both pulsed and frequency-domain (FD) modalities [4–7]. None of them presented a theoretical investigation which takes into account all the key effects of PA transient generation, acoustic attenuation, and the transducer transfer function. We introduced these factors in an analytical SNR evaluation and also performed experimental studies of these modalities [8]. In this manuscript, we expand the discussion on some features of both modalities, such as axial resolution and the choice of transducer bandwidth as well as incidence of laser light on the transducer and its consequences. We consider how these methods can be implemented in a clinical PA imager and optimize the results with regard to the characteristics of each method.

2 Theoretical and Experimental Comparisons

2.1 Theoretical FD Versus TD SNR

It has been shown that the theoretical SNR of TD versus FD-PA can be evaluated from [8]

$$\frac{SNR_{\mathrm{TD}}}{SNR_{\mathrm{FD}}} \leq \frac{B_{\mathrm{ch}}\left[\int\limits_{B_{\mathrm{T}}} \frac{\mathrm{e}^{-\alpha_{\mathrm{s}} f L}}{\mu_{\mathrm{a}} c_{\mathrm{a}} + \mathrm{j}\omega} \tilde{H}_{\mathrm{tr}}(f)\,\mathrm{d}f\right]^2_{\mathrm{real}}}{B_{\mathrm{T}}\left[\int\limits_{B_{\mathrm{ch}}} \frac{\mathrm{e}^{-\alpha_{\mathrm{s}} f L}}{\mu_{\mathrm{a}} c_{\mathrm{a}} + \mathrm{j}\omega} \tilde{H}_{\mathrm{tr}}(f)\,\mathrm{d}f\right]^2_{\mathrm{max.}}} \left(\frac{4E_0^2 B_{\mathrm{ch}}}{A_{\mathrm{I}}^2 T_{\mathrm{ch}}}\right), \tag{1}$$

where the SNR is the ratio of the power spectrum to the noise power [9], the tilde indicates the Fourier transform operation, c_{a} is the speed of sound, μ_{a} is the absorption coefficient, α_{s} is the acoustic attenuation, ω is the angular modulation frequency: $\omega = 2\pi f$, B_{ch} and B_{T} are the bandwidths of the chirp and ultrasonic transducer, respectively, E_0 is the pulsed laser intensity, A_{I} is the CW laser power intensity, T_{ch} is the chirp duration, L is the thickness of the medium over the absorber, and max. refers to the maximum of the real and imaginary components. H_{tr} is the transfer function of the transducer which can be characterized by some key properties such as the sensitivity, electrical impedance, and effective geometric features. The transfer function of the transducer can be added to the PA system model using the well-known Krimholtz–Leedom–Matthaei (KLM) model [8]. The difference in the FD and TD bandwidths and the effect of high-pass filtering in the pulsed method can be incorporated in the above formulation. However, the deterministic baseline which appears as a major fluctuation in the pulsed method was not incorporated in the formulation. Therefore, the formula can be considered as an upper limit of the SNR.

2.2 Experimental Setup and System Parameters

The strategy of this study is to characterize PA imaging by exploiting the capabilities and advantages of both CW and pulsed modalities under identical sample configuration

conditions and within the limitations the maximum permissible exposure (MPE) curve imposes [10]. Each method stands with its own features against a given imaging or absorber detection task. The employed dual-mode PA system was equipped with a pulsed and a CW laser, both 1064 nm [5,8]. The intensity modulation of the CW laser was implemented by an acousto-optic modulator (AOM) according to the waveforms defined in the software function generator. The experiments presented in this report were conducted with a 3.5 MHz focused ultrasonic transducer with a focal length of 2.54 cm. The LabView platform (National Instruments, Austin, TX) was used for function generation, signal acquisition, and processing. The energy level for the pulsed laser is specified in the ANSI standard [10] and was fixed at 100 mJ $\cdot$ cm^{-2} in the experiments.

3 Experiments and Results

The parameters of each modality were optimized to achieve the highest SNR. The FD excitation involves more controllable signal generation and detection parameters than pulsed excitation which were taken advantage of in this study. The FD-PA optimization was performed over key parameters: the frequency bandwidth, chirp duration, laser intensity, and number of averages [11]. It was shown that the optimal chirp bandwidth is not necessarily the ultrasonic transducer bandwidth [11]. For a 3.5 MHz transducer the chirp frequency sweep was set between 200 kHz and 3 MHz.

In the FD-PA, the number of averages and the chirp duration determine the exposure time, and the relation among the exposure time, intensity, and SNR is formulated according to the ANSI standard [8]. It is demonstrated that by decreasing the laser exposure time and increasing its intensity, the SNR and depth detectivity can be enhanced. Figure 1a compares the images of two absorbers 4 mm and 2 mm long located 22 mm inside a 0.47 % Intralipid solution in two situations: 6.5 W $\cdot$ cm^{-2} laser intensity and 800 ms laser exposure versus 15.6 W $\cdot$ cm^{-2} and 250 ms laser exposure. Here, the laser intensities in both cases correspond to the *MPE* standard. The ANSI limit for short exposure duration (100 ns $< t <$ 10 s) is calculated by $MPE = 1.1C_{\mathrm{A}}t^{1/4}$ [10], dividing that by the exposure time yields the maximum intensity. The coefficient C_{A} is equal to 5 for 1064 nm laser wavelength. It demonstrates the superior contrast of the right image corresponding to a higher power and shorter laser exposure time.

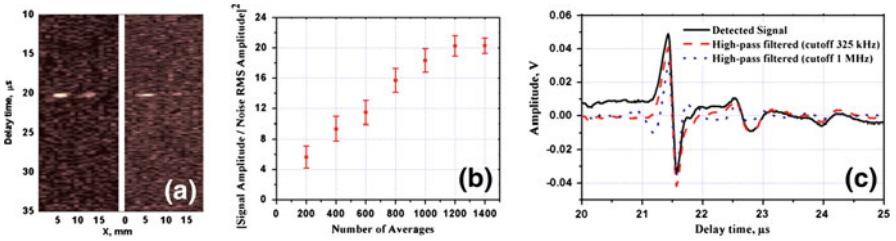

Fig. 1 (a) FD-PA images of two absorbers at 22 mm depth in a thick intralipid solution employing high power and short duration laser exposure (*left* 15.6 W $\cdot$ cm^{-2} and 250 ms) versus low power and long duration (*right* 6.5 W $\cdot$ cm^{-2} and 800 ms). (b) Signal-to-noise-amplitude (SNAR) increase by increasing the number of averages. (c) Pulsed transient before and after high-pass filtering. Cutoff frequencies were set to 325 kHz and 1 MHz

Equation 1 shows that the SNR of the FD-PA is proportional to the chirp duration, T_{ch}; experiments with chirp durations of 0.5 ms, 1 ms, and 2 ms support this conclusion [12]. However, by increasing the chirp duration, the laser exposure time is also increased. The maximum laser power exposure defined by tissue safety standards is the most crucial limitation in attaining a higher SNR. Therefore, it would be more appropriate to compare the SNR of different chirp durations at a constant total exposure time, in other words, to change the number of averages proportionally. It is well known that among a wide range of signal detection applications, by increasing the number of averages (N), one can enhance the SNAR proportional to $\sqrt{N}$ and the SNR proportional to N [13]. Therefore, it can be concluded that in the FD-PA, the combination of chirp duration and number of averages which is the total light exposure time should be considered. Figure 1b shows the linear increase in the square of SNAR with an increasing number of averages when the chirp duration is fixed. The SNAR increase does not continue after 1200 averages which demonstrates a saturation limit.

In contrast, to enhance the SNR in the pulsed mode, 30 averages were employed at each position. It is an experimental finding that performing around 10 averages for the pulsed transient at one location shows clear SNR improvement; however, more than 20 averages barely increase the SNR. This is due to the strong baseline which is deterministic, not random, and therefore is not eliminated (but becomes better delineated) by averaging. This is a major limitation of pulsed laser PA, resulting from the strong optical scattered fluxes during the pulse interacting with the transducer in back-propagation. To reduce the effect of baseline fluctuations, use of a high-pass filter was made [8]. Figure 1c compares the pulse-induced unfiltered transient with filtered signals with low cutoff frequencies of 325 kHz and 1 MHz. It shows that high-pass filtering reduces the baseline; however, it also demonstrates that by setting the cut-off frequency too high, the pulsed transient N-shape response will be distorted. Use of the wavelet-transform to reduce the baseline was also made [14, 15]; however, this kind of filter requires *a priori* knowledge of the signal profile.

Chirped FD-PA responses do not exhibit baseline interference effects, nor do they require high-pass filtering. The reasons are: (1) the limited chirp bandwidth acts as a bandpass filter by itself, (2) the lower power of FD-PA limits the signal power, therefore reducing the possibility of long reverberation of the transducer, and (3) the cross-correlation signal processing collects these unwanted signals to zero delay time. Figure 2 shows the pulsed and FD-PA signals from an absorber 1 cm below the surface of the intralipid solution. The effect of scattered laser light interaction with the

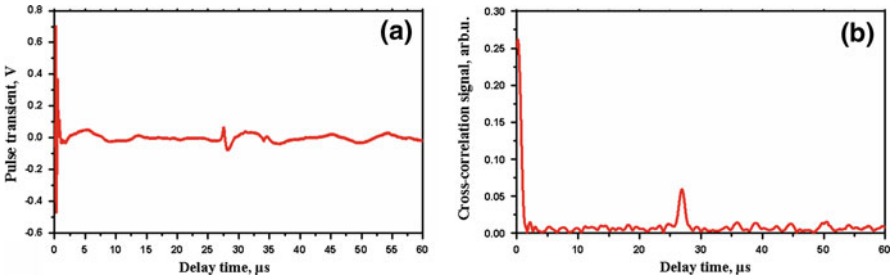

Fig. 2 Baseline fluctuation effect in (a) pulsed transient and (b) FD-PA signal trace

transducer dominates the whole TD signal trace, while the cross-correlation signal is affected within a very short interval of the delay time starting at zero.

The bandwidth of the PA system in the pulsed method is the maximum bandwidth of the transducer which could be much larger than the optimal bandwidth in the CW method. The difference in bandwidths is at the heart of the differences between the two modalities. In the pulsed PA mode, a laser pulse normally between 5 ns and 10 ns generates a very wide energy frequency spectrum in the 100 MHz to 200 MHz range. Here, the detector must respond to as wide a portion as possible of this launched wideband ultrasonic spectrum. This is the reason one seeks ultra-wide-band detectors in pulsed PA [16,17]. On the other hand, in FD-PA the user has the flexibility to select the energy spectrum, with optimal bandwidth in mind, such that it may produce the highest possible SNR under fixed optical energy deposition conditions. It should be mentioned that the optimal bandwidth for the SNR will not necessarily generate the best resolution. Although in pulsed PA, the best choice of bandwidth is the widest possible one; however, an added high-pass filter was shown to be beneficial to reducing baseline interference. These considerations also help to choose suitable transducers for each modality. For instance in the frequency range of 1 MHz to 5 MHz, despite the lower sensitivity of PVDF transducers, they could perform better for pulsed PA due to their wider bandwidth, while piezoceramics perform better for FD-PA due to their higher sensitivity.

Another experiment was designed to demonstrate the capability of both methods to recognize two depth-wise adjacent absorbers within a very close distance, a form of a Rayleigh axial resolution test. This experiment shows that although the full width at half maximum (FWHM) is a valuable measure of axial resolution in the pulsed and FD methods, for pulsed modality the effect of the bipolar shape (the negative part of the N-shape) should be considered as a limiting factor in the discussion of axial resolution to prevent any misleading. The first measurement was performed on a layer of a 1 mm thick plastisol strip separated from a thick plastisol piece by spacers. The axial distance between the top surfaces of the two plastisol pieces was $\sim$2.9 mm, and the absorption coefficient of both samples was 9 cm^{-1}. The sample was placed at a depth of 1 cm in the low-concentration intralipid solution (0.05 %). The A-scans are compared in Fig. 3a, b. Here, both pulsed and FD methods could distinguish separate inclusions. To enhance the axial resolution of the FD-PA, we combined (multiplied) the cross-correlation amplitude and the inverse of the standard deviation of the phase (ISDP) in Fig. 3c. In the next step, the absorbers were located closer together and the axial distance between the two plastisol pieces was $\sim$0.9 mm separated by transparent layers of tape. In Fig. 3d, the pulsed transient exhibits high resolution of both absorbers, however, with strong, and possibly confusing, baseline perturbations, while in Fig. 3e, the FD signal peaks from each absorber only partially overlapped. Figure 3f is the combination (multiplication) of the FD amplitude and ISDP signals [18]. The combination trace has the distinct advantages of an improved FWHM and a greatly suppressed baseline. The axial resolution (FWHM) of the peaks is shown in each of the traces of Fig. 3. While the FWHM in Fig. 3d is shorter than the delay time to the next peak, due to the bipolar shape of the pulsed signal, the second peak is difficult to distinguish.

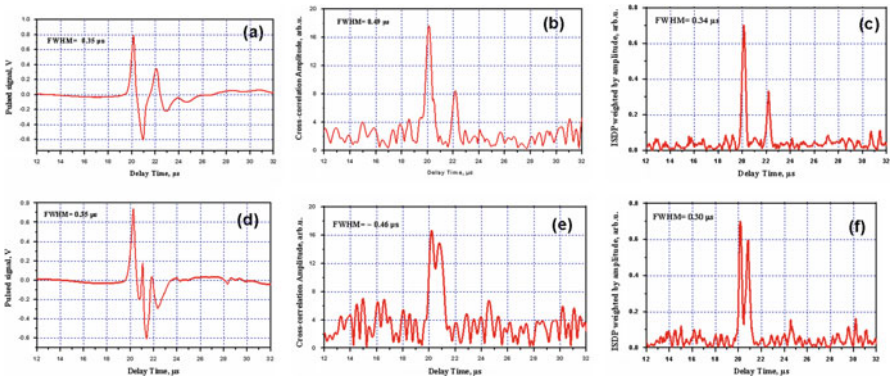

Fig. 3 Axial resolution comparison: (a) TD-PA, (b) FD-PA cross-correlation amplitude, (c) FD-PA: combining (multiplying) amplitude and ISDP channels for two adjacent absorbers ∼2.9 mm apart, (d) TD-PA, (e) FD-PA cross-correlation amplitude, and (f) FD-PA: combining amplitude and ISDP channels for two adjacent absorbers ∼0.9 mm apart

4 Conclusions

In this study, some features of the linear frequency modulated PA radar are compared with the conventional pulsed method. We adjusted the parameters of both modalities to achieve the maximum SNR using a dual-mode PA system within the safety standard for both modalities.

The SNRs of these methods were parametrically presented in terms of the transducer bandwidth, PA signal generation physics, and the laser pulse or chirp parameters. It was shown that the thermal transducer noise is not the only factor reducing the PA SNR, but in the pulsed modality, the baseline interference has a much stronger impact. Therefore, different strategies should be used to increase the SNR in these modalities. In conclusion, it has been described how parameters of the FD method can be adjusted to provide a SNR and resolution competitive with pulsed PA.

Acknowledgments The authors gratefully acknowledge the support of the Canada Foundation for Innovation (CFI), the Ontario Research Fund (ORF), and the Canada Research Chairs (CRC). They further acknowledge NSERC Strategic and Discovery Grants and the MRI Ontario Premier's 2007 Discovery Award in Science and Engineering to A.M.

References

1. Y. Fan, A. Mandelis, G. Spirou, I.A. Vitkin, J. Acoust. Soc. Am. **116**, 3523 (2004)
2. S.A. Telenkov, A. Mandelis, J. Biomed. Opt. **11**, 044006 (2006)
3. A.A. Oraevsky, A.A. Karabutov, Proc. SPIE **3916**, 228 (2000)
4. K. Maslov, L.V. Wang, J. Biomed. Opt. **13**, 024006 (2008)
5. S.A. Telenkov, A. Mandelis, J. Biomed. Opt. **14**, 044025 (2009)
6. S. Telenkov, A. Mandelis, Rev. Sci. Instrum. **81**, 124901 (2010)
7. A. Petschke, P.J. La Riviére, Biomed. Opt. Exp. **1**, 1188 (2010)
8. B. Lashkari, A. Mandelis, Rev. Sci. Instrum. **82**, 9 (2011)
9. M. Skolnik, *Introduction to Radar Systems* (McGraw-Hill, New York, 1962), p. 440

10. American National Standard for the Safe Use of Lasers, Standard Z136.1-2007 (American National Standards Institute, New York, 2007)
11. B. Lashkari, A. Mandelis, J. Acoust. Soc. Am. **130**, 1313 (2011)
12. B. Lashkari, Photoacoustic imaging using chirp technique: comparison with pulsed laser photoacoustics, Ph.D. Thesis, University of Toronto, 2011
13. J. Minkoff, *Signal Processing: Fundamentals and Applications for Communications and Sensing Systems* (Artech House Publishers, Boston, 2002), p. 167
14. R.O. Esenaliev, A.A. Karabutov, A.A. Oraevsky, IEEE J. Sel. Top. Quantum Electron. **5**, 981 (1999)
15. S.A. Ermilov, T. Khamapirad, A. Conjusteau, M.H. Leonard, R. Lacewell, K. Mehta, T. Miller, A. Oraevsky, J. Biomed. Opt. **14**, 024007 (2009)
16. A.A. Oraevsky, A.A. Karabutov, V.G. Andreev, R.O. Esenaliev, Proc. SPIE **3597**, 352 (1999)
17. V.G. Andreev, A.A. Karabutov, A.A. Oraevsky, IEEE Trans. Ultrason. Ferroelectr. Freq. Control **50**, 10 (2003)
18. B. Lashkari, A. Mandelis, Opt. Lett. **35**, 1623 (2010)